Analysis of the W.M. Keck Telescope
Primary Mirror Control Loop

J. Llacer, R.C. Jared, and J.M. Fuertes*
Engineering Division
Lawrence Berkeley Laboratory
University of California
Berkeley, CA 94720

*Facultat d'Informatica
Universitat Politecnica de Catalunya
08028 Barcelona, Spain

MASTER

Analysis of the W.M. Keck telescope primary mirror control loop

J. Llacer, R.C. Jared and J.M. Fuertes *

Engineering Division, Lawrence Berkeley Laboratory
1 Cyclotron Road, Berkeley, CA 94720
and
*Facultat d'Informatica, Universitat Politecnica de Catalunya
08028 Barcelona, Spain

ABSTRACT

The Primary Mirror Active Control System (ACS) of the W.M. Keck Telescope has as its main function the maintenance of the mirror figure of the 36-segment primary mirror under the changing effects of gravity, temperature, and other low frequency perturbations. The ACS is a multivariate control loop that can be represented in a diagonalized form, provided that segment actuator motions only excite oscillations in its corresponding whiffletree (tying an actuator to a mirror segment), with no coupling to the other whiffletrees in the same segment mirror. Since whiffletree oscillations are expected to occur at frequencies above the bandpass of the control system, the assumption is expected to be valid for the purpose of analyzing the stability and response of the ACS under the expected low frequency perturbations.

The results of a one-dimensional simulation, justified by the diagonalized form of the problem, will be presented showing the conditions for stability, the system response to desired changes and the advantages of using feed-forward. A verification of the theoretical results will be presented for an actual actuator coupled to a sensor controlled by a one-dimensional version of the ACS software.

Also based on the diagonalized form, a study of noise coupling, equivalent system bandwidth and matrix noise magnification factor will be presented. The effect of the feed-back control loop on the telescope rms image radius caused by sensor noise will be calculated.

1. THEORETICAL ANALYSIS

The W.M. Keck Telescope Primary Mirror Active Control System (ACS) has been described in a companion paper in this issue.[1] In this section we shall establish the theoretical basis for its analysis, a model for the ACS and conditions under which a simplified analysis can be carried out.

1.1 General Problem

The ACS is a multivariate control loop: the vector of inputs x and the vector of outputs y (see Fig. 1) are related by a matrix H that generally couples each element of x to some number of elements of y. The equation that defines the behavior of the simple system of Fig. 1 can be written as

$$H(x - y) = I \ y \qquad (1)$$

where I is the identity matrix. For the simple case of Fig. 1, vectors x and y have the same dimension, n, and, therefore, H is square and of dimension n x n.

Equation (1) can be rewritten as

$$Hx = (H + I)y \qquad (2)$$

and it represents the general statement that defines the behavior of the problem of Fig. 1.
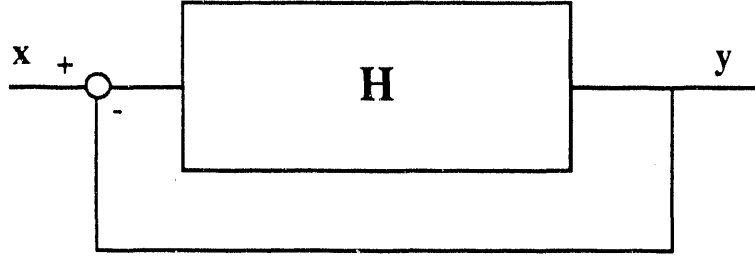
Fig. 1: Simple model of a multivariate control loop.

The direct analysis of Eq. (2) is very difficult, since matrix H has elements arbitrarily placed in its rows and columns. If the problem could be replaced by one in which all matrices are purely diagonal, as in

$$Du = D'v \qquad (3)$$

the analysis would be greatly simplified since each element of vector u would be only related to one element of vector v and the coupled problem would be reduced to a number of decoupled problems. We examine first the general procedure by which the replacement of problem (2) by problem (3) can be carried out.

1.2 Eigenvectors and eigenvalues of H and (H + I)

Let K_i be the ith eigenvector of H and K'_i the corresponding one of (H + I). Similarly, let λ_i be the ith eigenvalue of H and λ'_i that of (H + I). Their definitions are, respectively,

$$\left(H - \lambda_i I\right)K_i = 0 \qquad (4)$$

and

$$\left[(H + I) - \lambda'_i I\right]K'_i = 0 \qquad (5)$$

It will be convenient to rewrite the definitions (4) and (5) as

$$HK_i = \lambda_i I K_i \qquad (6)$$

and

$$(H + I)K'_i = \lambda'_i I K'_i \qquad (7)$$

Let us now postulate that the eigenvalues λ'_i can be represented as the sum of two eigenvalues λ_i and λ''_i in which the first one is the same eigenvalue of matrix H, as in (6), and λ''_i has to be determined.

With the new definition of λ''_i, Eq. (7) can be separated into two equations:

$$HK'_i = \lambda_i I K'_i \qquad (8)$$

and

$$IK'_i = \lambda''_i I K'_i \qquad (9)$$

Comparing (6) and (8) we recognize that K'_i equals K_i and an examination of (9) shows that λ''_i equals 1 for any vector K'_i. This finding indicates that the eigenvectors of H are the same as the eigenvectors of (H + I) and that the eigenvalues of H' are the same as those of H with the addition of 1 to each of them. With this knowledge, we can now proceed to diagonalizing the system matrices.

1.3 Diagonalization of H and (H + I)

A general matrix H can be diagonalized by the process

$$J^T H K = D \qquad (10)$$

where the matrix K has as its columns the eigenvectors of H and J^T has as its rows the eigenvectors of H^T. Since the eigenvectors of (H + I) are the same as those of H, matrices J^T and K will also diagonalize (H + I), i.e.,

$$J^T(H+I)K = D'. \tag{11}$$

The diagonal matrix D will have as its elements the eigenvalues λ_i of H, while D' will have the eigenvalues λ'_i, i.e., $(\lambda_i + 1)$. It follows that D' = (D + I).

Solving (10) and (11) for H and (H + I), and replacing in (2), we get

$$K D J^T x = K D' J^T y. \tag{12}$$

Removing K from both sides of the equation we are left with

$$D J^T x = D' J^T y. \tag{13}$$

Let us now examine $J^T x$. A vector x in the space spanned by matrix H can be represented as the expansion

$$x = u_1 K_1 + u_2 K_2 + ...$$

$$x = u_1 K_1 + u_2 K_2 + ... \tag{14}$$

where $u_i = \langle x, Y_i \rangle$, the dot product between vector x and the eigenvector Y_i of H^T.

The matrix J^T contains the eigenvectors of H as rows and, therefore, the product $J^T x$ will generate a vector u with elements u_i. Similarly for the right hand side of (13): the product $J^T y$ will generate a vector v with elements $v_i = \langle y, Y_i \rangle$. We are then left with

$$D u = D' v \tag{15}$$

which is a purely diagonal form, similar to the desired result of (3), relating the series expansions of x and y in a decoupled form.

We can summarize the results of this section with the following statements:

1) Eq. (2) relates the input and output vectors x and y through matrices H and (H + I) which are not diagonal.

2) Eq.(15) relates the series expansions u and v of the input and output vectors through matrices D and D' which are diagonal.

3) The basis vectors for the series expansions are the eigenvectors of H^T, the "natural modes" of the system.

4) The diagonal matrix D contains the eigenvalues of H in its diagonal and the matrix D' has the same elements with 1 added to the diagonal.

It is then possible to study system response, conditions for stability, etc., of the individual "natural modes" of the system in a totally uncoupled manner.

1.4 The error vector

In describing the behavior of a control system, the concept of an error vector defined as e = x - y is a very useful one, since it is usually the minimization of all the components of e that is desired. With the above definition of the error vector, Eq. (2) can be rewritten as

$$e = (H+I)^{-1} x. \tag{16}$$

In order to have e small for any possible value of x, it is necessary that all of its "natural mode" components be as small as possible. We have seen from (11) that the matrix (H + I) can be diagonalized by the matrices of left and right eigenvectors

J^T and **K**. Some algebraic manipulation starting from (11) shows that

$$(H + I) = K \, D' \, J^T \tag{17}$$

and, therefore

$$(H + I)^{-1} = K \, D'^{-1} \, J^T , \tag{18}$$

where $D' = (D + I)$ and **D** is the diagonal matrix of eigenvalues of **H**. Substituting into (16) we find

$$e = K \, D'^{-1} \, J^T x \tag{19}$$

which can be interpreted as follows:

$J^T x$, as discussed above, is a vector **u** containing the coefficients of the series expansion of **x** into its "natural modes". The product $D'^{-1} u$ modifies those coefficients by the characteristics of the control loop. Finally, the premultiplication by **K** brings the results back to the normal measurement space of **x**, **y** and **e**. If we now define an error vector in the "natural mode" space as **w** = **u** - **v̌**, (15) can be rewritten as

$$w = D'^{-1} u \tag{20}$$

which is equivalent to (19), but in the "natural mode" space. In order to minimize errors in all the "natural modes", it is then necessary that all the entries in the diagonal of D'^{-1} be small and uniform. If an entry, or group of entries, is large, errors in those corresponding modes will be significant. For those entries to be small and uniform, it is necessary that the entries of **D'** be large, i.e., (1 + eigenvalues of **H**) be large and uniform.

2. APPLICATION TO THE PRIMARY MIRROR CONTROL SYSTEM

2.1 Preliminary considerations

The control loop of the ACS can be looked at from two different points of view:

1) There is a set of 171 desired sensor readings **x** and a set of 171 actual sensor readings **y**. The error vector **e** is defined as **e** = **x** - **y** and the objective of the analysis is to evaluate **e** as a function of a perturbation vector **c** which is applied to the plant as a result of structure deformations and

2) There is a reference plane normal to the optical axis of the telescope. When the mirror attains its correct figure, each end of the 108 actuators is at a certain distance from the reference plane. The vector of these distances is a reference vector z_0. Under the influence of a perturbation vector **c** resulting from structure deformations, the actuator ends are at distances from the reference plane given by a vector **z**. The function of the control loop is to change the length of the actuators in order to bring **z** back to z_0. The error vector is **e** = z_0 - **z** and the objective of the analysis is to evaluate **e** as a function of the perturbations **c**.

The first formulation has an error vector and a matrix **H** of dimension 171 x 171 and the decomposition into eigenvalues and eigenvectors is carried out in the space of sensor positions. The second formulation has an error vector and a matrix of dimension 108 x 108, i.e., its decomposition is carried out in actuator position space.

An attempt at carrying out an analysis in sensor position space shows that the matrix **D** has only 108 eigenvalues in its diagonal different from zero, i.e., the matrix **H** is of rank 108, rather than 171. This is a consequence of the fact that the sensors in the ACS are not independent units, but their possible sets of positions are restricted to those generated by the possible sets of positions of the 108 actuators. It is correct, therefore, to work in the second formulation, with a matrix **H** of full rank.

2.2 A model for the ACS

The fundamental mathematical element of the ACS is the matrix **A** which relates actuator positions to sensor readings by the geometrical design factors of the primary mirror.[2] Its pseudo-inverse **B** is used in the control loop to calculate the correc-
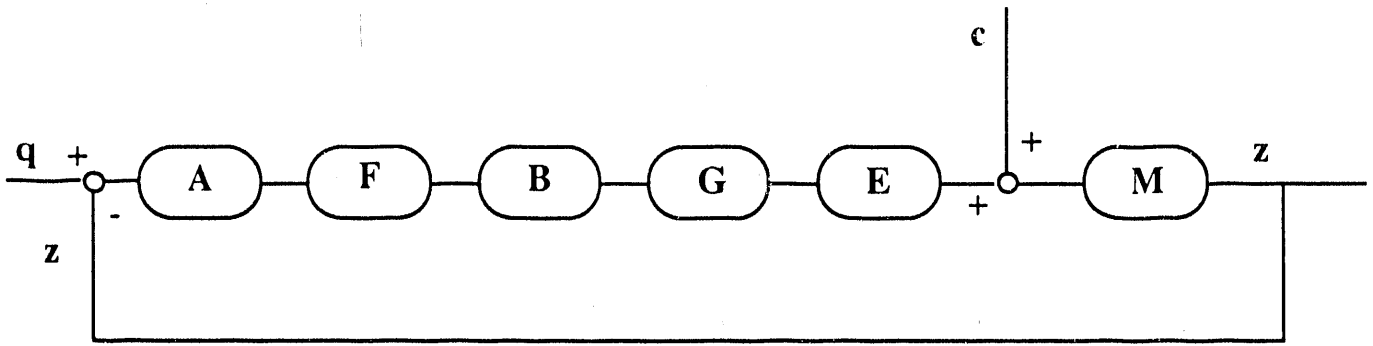
Fig. 2: Model of Keck Primary Mirror Control System. See text for description of components.

tions to be applied through the actuators when the sensor readings are not the desired ones for a given telescope attitude and temperature.

The model of the telescope that will allow us to carry out an analysis in the space of actuator positions is given in Fig. 2.

In the model, q is a general vector of desired actuator positions, which can be calculated for a set of desired sensor readings s_d by the equation

$$q = z_0 + B s_d. \tag{21}$$

Matrix A is a sparse matrix of dimension 171 x 108 that yields the changes in sensor readings from changes in actuator lengths. Matrix F is a diagonal 171 x 171 matrix containing the filter functions $f(s)$ for each sensor circuit as its non-zero elements. Here, s is the complex frequency variable. The ACS has been designed with a unique function $f(s)$, so that all diagonal elements are identical. Matrix B is the pseudo-inverse of A, which converts sensor readings back to actuator lengths. Matrix G is the gain matrix, which, for a single gain parameter for the complete system becomes $G = gI$. The matrix E is the matrix of actuator mechanical responses to an electrical impulse input, with entries which are functions of s. Actuators do not all respond in the same way to identical electrical inputs, but we have considered the responses sufficiently similar that they can be represented by a single function. Then, $E = e(s)I$. Finally, matrix M contains the mechanical response of the whiffletrees to actuator output impulses. We assume initially that an actuator motion will only excite oscillations in its corresponding whiffletree, with no coupling to the other whiffletrees in the same mirror or in other mirrors. For that simple case, we have a diagonal matrix, $M = m(s)I$.

The perturbation $c(s)$ is due to effects of gravity and temperature on the telescope structure and it is the principal disturbance of the system. We define the error vector

$$e = q - z \tag{22}$$

and we want to obtain an expression for e as a function of the perturbation c. The resulting expression is

$$-e = [I + MEGBFA]^{-1} Mc \tag{23}$$

which has the same form as (16) and can be treated identically for the analysis of the problem. However, with the simple definitions given above, realizing that $BA = I$ to very high accuracy, the expression becomes

$$-e = [1 + megf]^{-1} Imc \tag{24}$$

or

$$-e = \left[\frac{m}{1 + megf} \right] c \tag{25}$$

5

with all the terms being possibly functions of the complex frequency variable s.

The design decision of using only one kind of filter in all 171 sensor elements has resulted in the product BFA of (23) being purely diagonal. The simplifying assumption that whiffletrees are not coupled among each other makes M also purely diagonal and we end with a system represented by an uncoupled set of equations that relate the error in an actuator length to the gravity and temperature deformations on that specific actuator.

The problem of stability analysis, filter design and application of feed forward becomes very reasonable with the system defined by (25). The effects of whiffletree couplings can be left out for those aspects of the design because whiffletree resonances are expected to occur at frequencies substantially above the band pass of the filter f, where attenuation is expected to be very high. The control loop is not expected to respond to those oscillations.

A more complete analysis of the system would require placing off-diagonal terms in M and diagonalizing the problem following the methods described in the earlier part of this paper. Similarly, couplings between actuator motions through the support structure can be studied by placing off-diagonal terms in matrix E. The analysis would have to be carried out in terms of the natural modes of the system and it is beyond the scope of the present work. A study of such nature has been reported in Ref. 3.

3. ONE-DIMENSIONAL SIMULATION OF THE ACS

3.1 Software simulation

With the decoupled formulation of the ACS of (25), it is possible to study the behavior of the control loop with a one-dimensional simulation. This has been carried out by writing a computer program that studies the relationship among single corresponding elements of the input, output, gravity deformation and other vectors. In order to include in the study the effects of sampling, the simulation program runs in pseudo-real time, i.e., there is a software clock that generates time marks representing 100 Hz ticks (the data acquisition rate of the mirror system) and a set of C-language structures define timers, interrupt generators, flags, etc., so that different parts of the program can act when it is their time, with timing relationships that are well defined. The loop is closely related to that of Fig. 2 and is shown in Fig. 3.
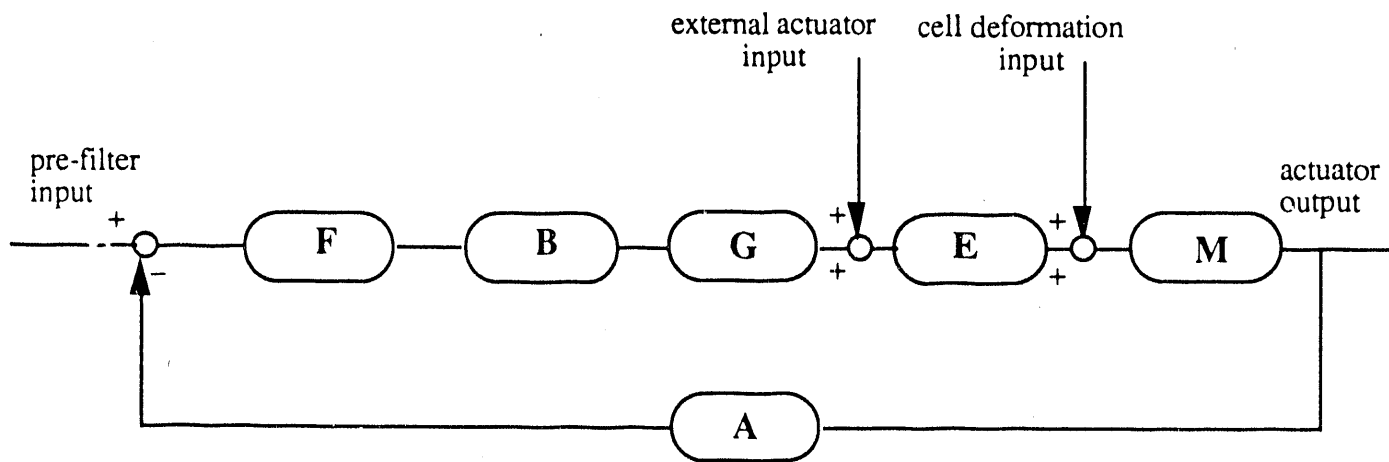

Fig. 3: Model for the one-dimensional simulation of the Keck Primary Mirror Control System.

The elements of Fig. 3 are the following:

F   The control filter. Four types of recursive filters have been simulated: single pole on the real axis, double pole on the real axis, a two-pole Butterworth and a two-pole Cauer.

B   The B matrix. We have taken the value of unity as the transformation of this element, except that the output of B appears delayed with respect to its input by a specified matrix multiplication time.

G   A gain parameter, consisting of a simple multiplication.

E   The response function of the single actuator of the system. An input value to E is picked up at a 2 Hz time mark (the update rate of the control loop). This initiates the move of the actuator, with the output representing its length as a function of time. An approximate actuator behavior has been simulated by making the move at two velocities for moves larger than 100 nm: all but the last 100 nm are done at 25000 nm/sec, while the last portion is done at 1000 nm/sec. For shorter moves only the slower velocity is used.

M   Mechanical response of the whiffletree structure. It has been set equal to unity.

A   The response of the mirror system, which has been set equal to unity. In this simulation, a single actuator motion will appear as a reading of the same length at the single sensor.

Important parameters that have been used in the simulations are:

a)   Pre-filter input: A desired motion request applied before the input summing point.
b)   Filter ouput: The output of F.
c)   External actuator input: A signal that is applied from outside the loop for feed-forward.
d)   Actuator length: Integrated output of all actuator moves during a simulation, available at the output of E.
f)   Cell deformation input: Effect on the apparent length of the actuator caused by deformations of the telescope cell by gravity during star tracking or fast slewing, or by temperature changes.
g)   Sensor output: Identical to actuator length in this simulation, available as output of A.

3.2 Hardware simulation

For the purpose of verifying the correctness of the software simulation described above, a one-dimensional form of the ACS control loop has been setup in real hardware. One actuator[4] physically connected to one sensor[5] have been controlled by portions of the ACS multiprocessor hard- and software in order to measure actuator positions as a function of time after the request for a step motion, with and without the application of feed-forward. A schematic of the functions implemented is shown in Fig. 4.

During operation, the system was allowed to reach steady state at an arbitrary sensor reading before applying a step input. After the steady state was reached, a step of 1000 nm in desired sensor reading was applied and the output of the filter, the actuator move size, actuator length and sensor readings were recorded as functions of time for a period of 40 sec. The measurements were repeated for the case in which a feed-forward step was also applied directly to the actuator through the software determining the move size. For the feed-forward case, a delay of 0.12 sec. existed between the application of the feed-forward step and the corresponding step in the desired sensor readings. This time delay is approximately one half of the time needed by the actuator to complete a move. Its application results in the reduction of the disturbance to the system as a result of applying the feed-forward step. A real-axis double pole cascaded filter with a cutoff frequency $f_c = 0.2$ Hz was used in the measurements and loop gains of 0.1 and 0.2 were investigated. The parts of the system that run at 100 Hz are shown in thin lines, those in thick lines run at 2 Hz.

3.3 Comparison of hardware and software simulations

Figure 5 shows the sensor readings calculated by the computer program and the results of the hardware measurements for the one-dimensional simulation of the ACS in response to a request of a change in sensor readings of 1000 nm, for loop gains of 0.1 and 0.2, no feed forward.

The results of Fig. 5 show a slight discrepancy in the shape of the responsed curves which we attribute to the uncertainty in the value of the experimental actuator and sensor conversion factors of electrical signals to motion nm and to the assumptions made in the software simulation regarding matrix multiplication times and actuator motion profiles.

Figure 6 shows comparisons of the hardware and software response curves when a feed-forward signal is applied directly to the actuator system input. The case shown in the figure corresponds to a desired change in sensor readings of 1000 nm but with an actual feed-forward signal of 1010 nm, simulating a 1% error in the knowledge of the conversion factors between
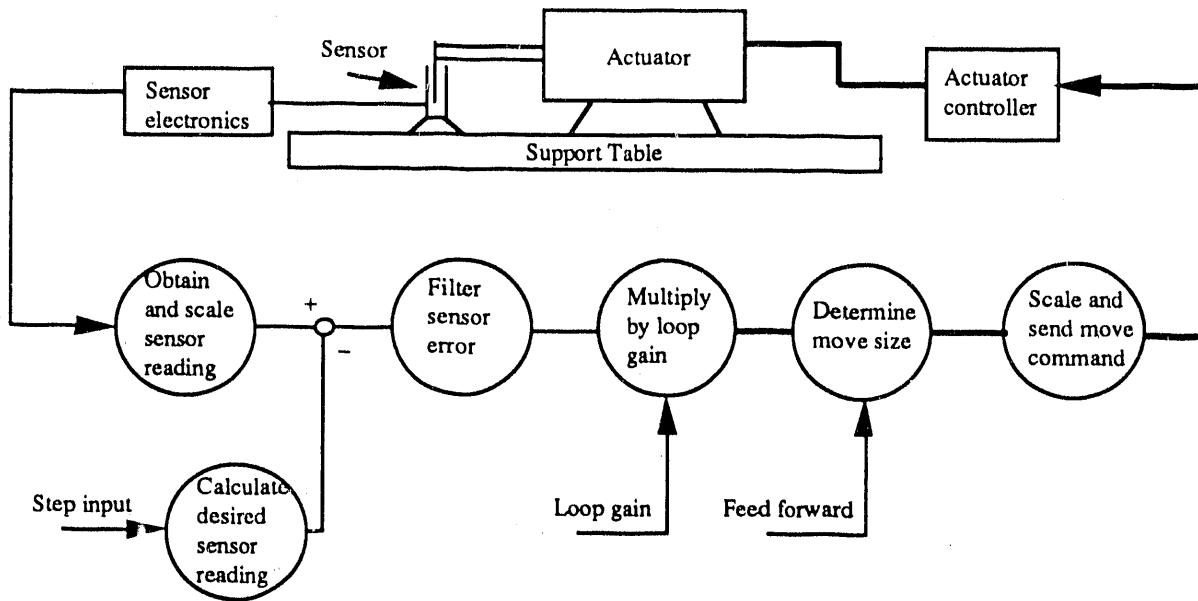
Fig. 4: Schematic of the portion of the ACS used for verification of software simulation.
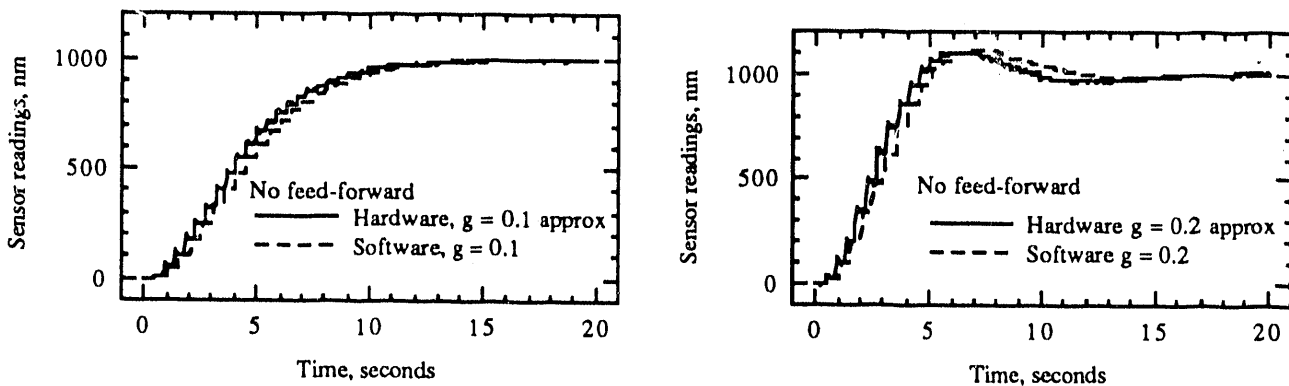

Fig. 5: Comparison of hardware and software one-dimensional simulations, without feed-forward.

actuator travel and drive magnitude. The rapid achievement of the desired sensor reading is observed, although there is a settling time in both the hardware and software results which depends on gain. The magnitude and sign of the error in the first few seconds after the feed-forward signal is applied is found to depend on the size of the delay in applying the desired sensor values to the pre-filter input of Fig. 3 (step input of Fig. 4) after the feed-forward signal is applied. In principle, this error can be reduced to zero if actuator move profiles were known exactly.

Having checked that the computer simulation is adequate to represent the one dimensional version of the ACS, a large number of parameters have been examined in order to study their effect on control loop performance. We will show here only the results corresponding to determining maximum loop gain before instability and the optimum settings for fastest recovery from a fast, large change in azimuthal angle when scanning the sky.

Figure 7 shows the results of the software simulation of the ACS control loop with gains above the expected points of operation. With a gain g = 0.5 the loop is underdamped, resulting in long oscillations about the desired point. When g is increased to the neighborhood of 1.15, we are reaching the instability point, in which the oscillations do no longer decay. At g > 1.25 the control loop becomes an oscillator.
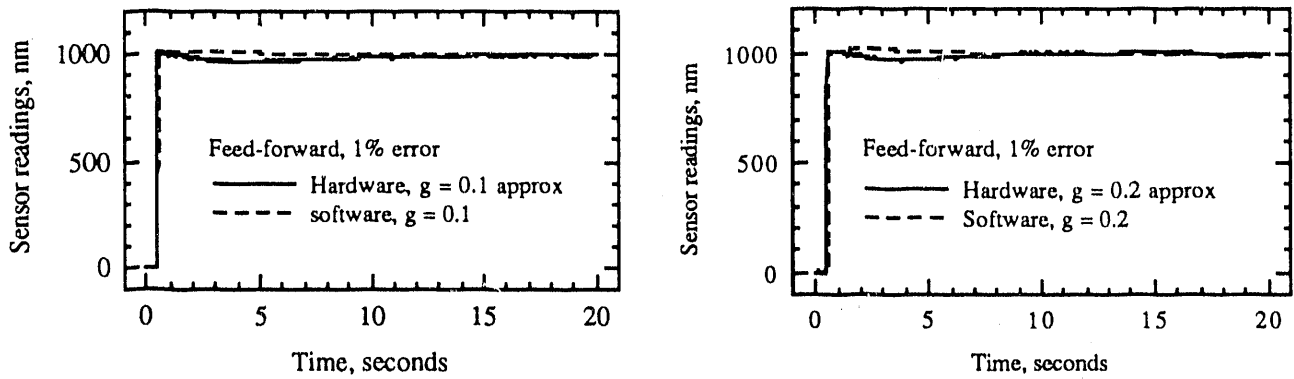
8

Fig. 6: Comparison of hardware and software simulations with feed-forward. An error of 1% is assumed to exist in the calibration of the actuators.
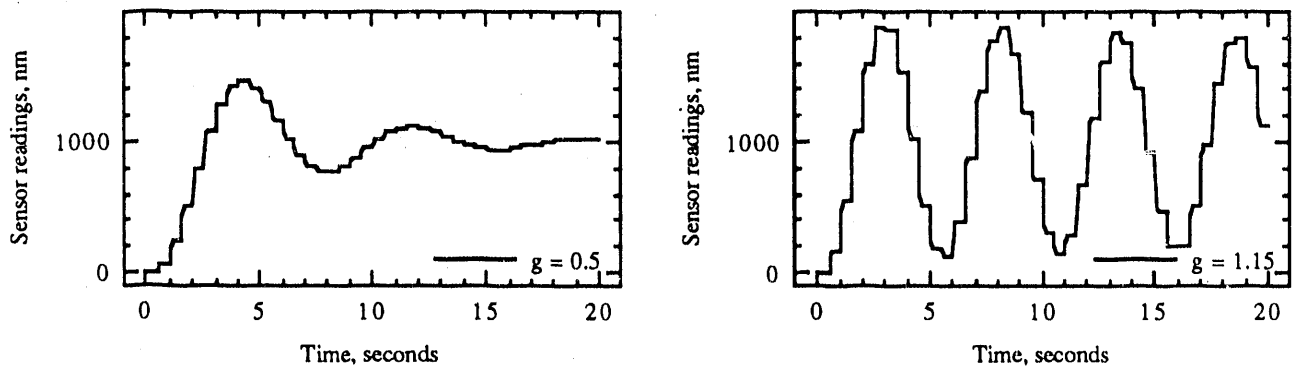

Fig. 7: Step response of the one-dimensional software simulation of the control loop with gains of 0.5 and 1.15. The first is for an underdamped loop and the latter corresponds to a nearly unstable loop.

Figure 8 shows the behavior of the ACS software simulation during and after a fast slewing move at 2500 nm/sec, as would occur when the telescope has to move from one point of the sky to another with a minimum loss of time.

Figure 8, left, shows the sensor readings during the five seconds of the motion, followed by the readings during settling. The graph at the right shows a magnification of the sensor readings scale during the settling time. With reference to Fig. 3, the slewing motion was simulated as follows:

a) pre-filter input = 0 - the desired sensor readings were 0 at all times.

b) cell deformation input = a ramp of 2500 nm/sec, corresponding to maximum apparent shortening of an actuator under gravity forces during fast slewing.

c) external acuator input = a pulse of 1275 nm applied at 2 Hz corresponding to a feed-forward signal with a 2% error in the knowledge of the actuator conversion factor between electrical signals and actual motion.
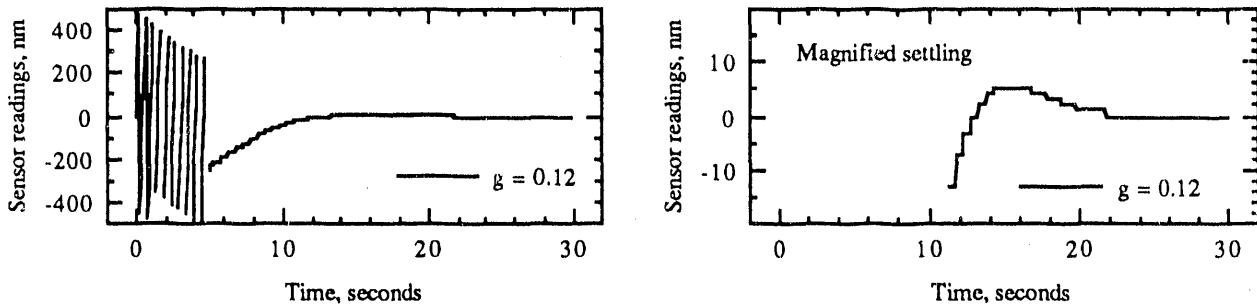
9

Fig. 8: Settling of the ACS software simulation after a fast 5 second move of 2500 nm/sec. The graph on the right shows a magnified view of the sensor reading scale during the final settling of the system.

The oscillatory behavior of the sensor readings during the fast move is due to the fact that the feed forward signal is applied as discrete steps at 2 Hz, while the cell deformation input is a ramp. The final value of the ramp is identical (to within the conversion factor error) to the integral of the feed-forward steps, but oscillations occur during the process. The settling time would be zero if the actuator (and sensor) conversion factors were known exactly and the exact time of application of the feed-forward signals with respect to the cell deformation input and the profile of actuator moves could be determined exactly. Then, the net energy stored in the filters at the end of one loop cycle (0.5 sec) would be zero. For an expected error in conversion factors of 2% and a first order approach to the feed-forward step timing, the simulation shows a settling time of ~ 7 sec to within 10 nm of the final desired sensor reading. A gain of 0.12 was selected as the approximate value that resulted in fastest settling time.

4. SENSOR NOISE ANALYSIS

4.1 General analysis

For a system like the ACS, a general noise analysis has to take into account the fact that the transfer functions and feedback functions are matrices, so that each element of the output vector may be connected to some or all of the inputs. A treatment of this type of system can be found in Ref 6. The relationship between the power spectral densities of each output element y_i and that of the input elements x_j is given by

$$S_{y_i}(f) = \sum_{j=1}^{J} |H_{ij}(f)|^2 S_{x_j}(f) \qquad (26)$$

where $S_{y_i}(f)$ is the power spectral density of the ith ouput, $S_{x_j}(f)$ is the density of the jth input and $H_{ij}(f)$ is the transfer function between the jth input and the ith output. This is for the case with inputs x_j uncorrelated.

The transfer function of the feedback system of Fig. 3, simulating the Keck ACS, can be studied by making reference to the more general problem exemplified by Fig. 9, in which x and y are input and output vectors, respectively, and h and f are the impulse response function matrices of the main transfer and feedback elements.

In order to obtain the multivariate transfer functions, we define the autocorrelation function

$$R_{y_i}(t_1, t_2) = E\{y_i(t_1)y_i(t_2)\} \qquad (27)$$

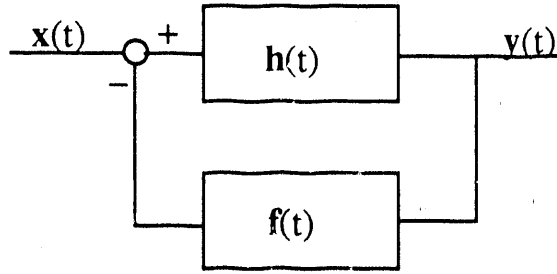where E{ } indicates expected value. For the general system of Fig. 9,

10

Fig. 9: General multivariate feedback system.

$$y_i(t) = \sum_j \int_{-\infty}^{+\infty} h_{ij}(\lambda) \, x_j(t-\lambda) \, d\lambda - \sum_j \sum_l \int_{-\infty}^{+\infty}\int_{-\infty}^{+\infty}\int_{-\infty}^{+\infty} h_{ij}(\lambda) \, f_{jl}(\gamma) \, y_l(t-\lambda-\gamma) \, d\lambda \, d\gamma \, dt \qquad (28)$$

Fourier transforming both sides, and letting capital letters stand for the transforms of the corresponding small case letters, we obtain

$$Y_i(f) = \sum_j H_{ij}(f) \, X_j(f) - \sum_j \sum_l H_{ij}(f) \, F_{jl}(f) \, Y_l(f) \qquad (29)$$

In the relationship of Eq. 29, the second term of the right hand side (due to the feedback element) contains all the elements of the output vector Y and there is no general solution for the transfer function relating one single $Y_i(f)$ to the input vector $X(f)$. For the ACS case, with the simplifying definitions given in Sect. 3.1, the situation is much better.

The elements of the matrix H in (29) correspond to $M(f)E(f)G(f)F(f)B$ in the ACS (compare Figs. 3 and 9), i.e., each element of the pseudo-inverse matrix B is multiplied by the product of transfer functions indicated. Matrix F of (29) corresponds to the matrix $A(f)$, sparse, non-diagonal, in the ACS.

With these substitutions and letting $C(f) = M(f)E(f)G(f)F(f)$, (29) becomes

$$Y_i(f) = C(f)\sum_j b_{ij} \, X_j(f) - C(f)\sum_j \sum_l b_{ij} \, a_{jl} \, Y_l(f) \qquad (30)$$

Since B is the pseudo-inverse of A, the summation over j in the second term of the right hand side of (30) results in 1 for $i = l$ and 0 otherwise. We are then able to solve for $Y_i(f)$:

$$Y_i(f) = \left\{ \frac{C(f)}{1+C(f)} \right\} \sum_j b_{ij} \, X_j(f) \qquad (31)$$

The transfer function relating one output Y_i to all the inputs X_j needed to calculate the output power spectral densities of (26) can then be obtained from (31).

4.2 Noise coupling in the ACS

For the simplified feedback system of the ACS, as described in Sect. 3.1, the power spectra of the output noise as a function of the input power spectra can be obtained from (26) and (31). The result is

11

$$S_{y_i}(f) = \left| \frac{C(f)}{1 + C(f)} \right|^2 \sum_j |b_{ij}|^2 \, S_{x_j}(f) \tag{32}$$

An examination of (32) shows that the noise power of the ith output contains a contribution from all the input noise powers, with coupling coefficient given by the squares of all the elements of the rows of the B matrix. If we consider identical noise sources at all inputs, the summation of the square of the elements of the rows of the B matrix represents a noise magnification ratio which will be evaluated below. The first term of (32) represents the effect of the transfer function of the system. Its integral over all frequencies results in the equivalent noise bandwidth of the system with feedback, for noise sources that are essentially flat in the bandwith of the system.

4.3 Equivalent system bandwidth

With the simplifying approximations described in Sect. 3.1, the function $C(f)$ of (32) is simply the frequency response of an integrator (the actuator) and two single pole cascaded filters. The equivalent system bandwidth has been obtained by integrating numerically the first term of (32) over all frequencies and is given in Table I.

TABLE I

Equivalent System Noise Bandwidth with Double Pole Filter, $f_c = 0.2$ Hz

Loop Gain g	Eq. Bandwidth (Hz)
1.0	0.31
0.25	0.108
0.10	0.048

4.4 Matrix noise magnification factor

With the assumption that all noise sources are identical and independent, the matrix noise magnification factor obtained from (32) has components that range from 3.31 rms at actuators belonging to the more tightly coupled mirrors to 8.06 rms for some of the actuators in peripheral mirrors. The rms noise magnification for the complete primary mirror is found to be 4.75. It can be interpreted as the factor by which the rms noise that could be measured at the output of a sensor is magnified when measured at an actuator site, with all the sensors and actuators in operation.

4.5 Primary mirror image rms noise

The rms image radius for noise generated at the sensors is defined by

$$\theta_{rms}^2 = \frac{1}{M} E \left\{ \sum_{m=1}^{M} |\theta_m|^2 \right\} \tag{33}$$

where M is the number of mirror segments, θ_m is the deviation angle from the perfect mirror ray and $E \{ \}$ is the expected value. Mast and Nelson have obtained a formula for that value for the primary mirror of the Keck telescope in terms of a sensor noise σ_s. Their result, Eq. 22 of Ref. 2, is

$$\theta_{rms}^2 = \left(\frac{4}{3t}\right)^2 \left(\frac{\sigma_s^2}{4}\right) \frac{1}{M} \sum_{m=1}^{M} \sum_{k=1}^{3} \sum_{k'=1}^{3} \sum_{n=1}^{N} \left(B_{(km)n} - B_{(k'm)n} \right)^2 \tag{34}$$

12

where the (km) index on B refers to row i of the matrix B and $i = 3(m-1)+k$ for the kth actuator on the mth segment, N is the number of sensors and M is the number of mirror segments, as above.

It will be interesting to see how (34) is affected by the feedback nature of the control loop and its limited bandwidth. For that purpose we start with Def. (33), interchanging expectation and summation. Using the expression for the image angle of a mirror ray in terms of actuator lengths p, given by Eq. 13 of Ref. 2 , we obtain

$$\theta^2_{rms} = \frac{1}{M} \sum_{m=1}^{M} E\left\{\theta^2_m\right\} = \frac{1}{M}\left(\frac{4}{3t}\right)^2 \sum_{m=1}^{M} E\left\{p^2_{1m} + p^2_{2m} + p^2_{3m} - p_{1m}p_{2m} - p_{2m}p_{3m} - p_{3m}p_{1m}\right\} \tag{35}$$

In the notation of the present paper, $p_{km} = y_i$, where $i = 3(m-1) + k$, i.e., y_i is the length of the ith actuator. The expected value of the quadratic terms y_i^2 can be obtained from

$$E\left\{y_i^2\right\} = E\left\{y_i(t)\,y_i(t+\tau)\right\}_{\tau=0} = R_{y_i}(t,t+\tau)\big|_{\tau=0} = \int_{-\infty}^{+\infty} S_{y_i}\,df = \int_{-\infty}^{+\infty}\left|\frac{C(f)}{1+C(f)}\right|^2 \sum_j b_{ij}^2\, S_{x_j}(f)\,df \tag{36}$$

where R is the autocorrelation function and S is the power spectral density, given by (32). The integral at the right hand side of (36) for a sensor noise spectrum which is flat within the band pass of the control system and of value σ_s^2 per unit bandwidth, with all the sensors identical and independent, becomes

$$E\left\{y_i^2\right\} = BW_n^2\, \sigma_s^2 \sum_j b_{ij}^2 \tag{37}$$

where BW_n is the equivalent noise bandwidth at the loop gain employed. For the cross terms in (35), a similar treatment shows that

$$E\left\{y_i y_l\right\} = BW_n^2\, \sigma_s^2 \sum_j b_{ij}b_{lj} \tag{38}$$

Substituting (37) and (38) into the expression for the rms image radius of (35), and after some algebraic manipulation and changing back to Mast and Nelson's notation, we obtain

$$\theta^2_{rms} = \left(\frac{4}{3t}\right)^2 \frac{1}{4M} \sum_{m=1}^{M}\sum_{k=1}^{3}\sum_{k'=1}^{3}\sum_{n=1}^{N}\left(B_{(km)n} - B_{(k'm)n}\right)^2 BW_n^2\, \sigma_s^2 \tag{39}$$

This equation is nearly identical to the result of Mast and Nelson, the only difference being the appearance of the effective noise bandwidth factor.

The implications of (39) are that, for noise sources that are essentially white within the ~ 0.2 Hz bandpass of the control loop, the value of σ_s (in nm/Hz$^{1/2}$) that has to be used in calculating the rms image radius has to be multiplied by the effective noise bandwidth, which is gain dependent and lower than unity for the ACS, as seen from Table I. For noise sources whose energy can be approximated by a δ-function at very low frequencies, the value of the corresponding factor is essentially $g/(1 + g)$, so that their effect is also reduced by using a feedback control loop at low gain. In all cases, however, the mechanism for noise magnification by coupling by matrix terms is present.

5. CONCLUSIONS

This paper has focused on two aspects of the Primary Mirror Control System of the Keck Telescope. The first has been a study of the time response of the system to desired changes in mirror figure, or to the ability to maintain a specific mirror figure under the changes due to gravity and temperature during star tracking or fast slewing. The second aspect has been a study of the noise magnification effects of the control matrix B and the equivalent noise bandwidth of the feedback loop forming the ACS. In the process of carrying out both studies, it has become evident that the simplified case in which the matrix M of mechanical whiffletree response of Fig. 3 is diagonal, leads to a simplified problem that can be treated with reasonable ease. That assumption is expected to be true for the ACS in the bandpass frequencies of the system. If after working with the telescope it is found that the assumption does not hold sufficiently well, this paper has laid out the methods by which a more complete study can be carried out. The study of the dynamic behavior would start from (20) and the study of noise coupling would start from (29). The results found in this paper can be summarized as follows:

1) With the filter cut-off frequency specified at 0.2 Hz by the need to remove aliasing of higher frequency oscillations of the mechanical system, the expected range of operating loop gains can be expected to be between 0.1 to 0.2, depending on the operation.

2) The phase lag introduced by the filter necessitates the use of feed-forward, which can bring settling time to less than 10 seconds in all tested cases of interest.

3) The fact that the ACS is a feedback control loop operated at a low gain, results in a reduced noise measured at the actuators given by the sensor input noise times a factor that ranges between the effective noise bandwidth of Table 1 and $g/(1 + g)$, depending on the spectrum.

4) The fact that the control matrix B couples each actuator to all the sensor noise sources results in an rms noise magnification ratio of 4.75, independent of power spectrum. Factors 3 and 4 have to be considered together in calculating the system noise.

5) The rms image radius calculated by Mast and Nelson can be reproduced by the analysis of the present paper, provided that the value of σ_s used is multiplied by the equivalent noise bandwidth at the operating gain. It is also evident that that analysis only holds for the case of a diagonal mechanical whiffletree response matrix. If the assumption is not applicable in the bandpass of the ACS, higher noise can be expected than the one now calculated.

6. ACKNOWLEDGMENTS

7. REFERENCES

1. R.C. Jared et al, "The W.M. Keck Telescope Segmented Primary Mirror Active Control System," in this issue.

2. T.S. Mast and J.E. Nelson, "The Figure Control of Segmented Telescope Mirrors," Keck Observatory Report No. 80.

3. J-N. Aubrun, K.R. Lorell, T.W. Havas and W.C. Henninger, "An analysis of the segment alignment control system for the W.M. Keck Observatory ten meter telescope," Keck Observatory Report No. 143.

4. J.D. Meng et al, "Position actuators for the primary mirror of the W.M. Keck Telescope," in this issue.

5. R.H. Minor et al, "Displacement sensors for the primary mirror of the W.M. Keck Telescope," in this issue.

6. W.B. Davenport and W.L. Root, *Random Signals and Noise,* McGraw-Hill Co., 182-185 (1958).

END

DATE FILMED

12 / 19 / 90